Closed-loop separation control: An analytic approach

M.-R. Alam, W. Liu,[a] and G. Haller[b]
Department of Mechanical Engineering, Massachusetts Institute of Technology, 77 Massachusetts Avenue, Cambridge, Massachusetts 02139

(Received 1 June 2005; accepted 22 February 2006; published online 3 April 2006)

We develop an analytic approach to two-dimensional flow separation control by feedback. With two wall-based actuators enclosing an array of distributed wall-shear sensors, we control the wall-shear evolution equation through its boundary values at the actuators. Using this approach, we induce separation at prescribed locations in steady and unsteady channel flows, and reduce the recirculation length behind a backward-facing step to a prescribed value. © *2006 American Institute of Physics*. [DOI: 10.1063/1.2188267]

I. INTRODUCTION

Separation control alters the location and extent of flow detachment from a no-slip boundary to increase lift, improve pressure recovery, or reduce drag. Modern approaches focus on exciting large-scale coherent structures in the flow through flaps, synthetic jets, plasma actuators, speakers, or other devices (see Greenblatt and Wygnanski[1] for a comprehensive review).

Open-loop control strategies, such as periodic blowing and suction, are successful in delaying separation or facilitating reattachment.[2–7] The best placement and frequency of the actuators, however, is problem specific, and is typically optimized with respect to a small number of parameters. As a result, successful open-loop strategies do not necessarily carry over to different flow conditions and geometries. On a more general note, it is not broadly understood why particular actuation mechanisms work.[8]

For closed-loop separation control, a simplified model of the separated flow physics appears essential. Well-performing models include one-degree-of-freedom damped linear oscillators,[9] vortex-based models,[10,11] low-dimensional Galerkin truncations,[12,13] self-tuning linear black-boxes,[14] and nonlinear plants with an unknown steady component explored on-line.[14] The controllers using these models, however, still use open-loop-optimized forcing frequencies amid varying closed-loop flow conditions. In addition, available separation controllers rely on Prandtl's steady separation theory[15] while seeking to control highly unsteady flows.

Arguably, an ideal closed-loop separation controller would target large-scale unsteady flow structures by locally actuating their point of contact with the flow boundary. For no-slip boundaries, such a controller was developed by Wang *et al.*[16] In that reference, the authors used feedback linearization at the wall to control wall-based Lagrangian coherent structures (unstable manifolds) along which fluid particles are ejected from the wall.

The above feedback linearization scheme fails for viscous flows, because no-slip boundary conditions make the particle dynamics near the wall inherently nonlinear. A recent *kinematic theory* of unsteady separation[17,18] has, however, revealed that separation from no-slip walls is also governed by unstable manifolds, except that they are *nonhyperbolic*: their location cannot be identified from linearization. While such manifolds remain hidden in instantaneous streamline, vorticity, and pressure plots, they are readily seen in flow-visualization experiments as sharp material spikes emanating from the wall.[19]

Using the above kinematic theory, one can construct a closed-loop algorithm for controlling unsteady separation in two-dimensional time-periodic Stokes flows.[20] The algorithm includes a delay effect arising from the finite distance between the wall-based actuators and the intended separation point. While the resulting controller works accurately for linear model flows, the algorithm assumes the wall-shear field to be a linear superposition of the uncontrolled wall shear and the actuator wall shear. Numerical simulations invalidate such an assumption for Navier-Stokes flows, even in the low-Reynolds-number regime.

Motivated by the success of the above kinematic controller for Stokes flows, here we develop a general closed-loop algorithm for controlling the location of unsteady separation and reattachment in two-dimensional Navier-Stokes flows. Our controller enforces the exact kinematic separation criteria[17,18] and hence creates wall-based unstable manifolds at prescribed locations. The underlying control algorithm is based on the exact wall-shear evolution equation, a one-dimensional nonlinear partial differential equation (PDE) defined on the wall between two discrete actuators.

By observing the nonlinear term of the wall-shear PDE directly from the flow, we reduce the separation control problem to the two-point boundary control of a one-dimensional heat equation. Feeding back the error of the kinematic separation criteria at the prescribed separation location, we obtain explicit expressions for the required discrete actuation strengths. We prove that this procedure does induce separation at the desired location as long as the controlled velocity flow admits uniformly bounded derivatives.

We implement the above control principle in closed-loop numerical simulations of two-dimensional Navier-Stokes

[a]Present address: Department of Mathematics, University of Central Arkansas, 201 Donaghey Avenue, Conway, AZ, 72034.
[b]Author to whom correspondence should be addressed. Electronic mail: ghaller@mit.edu

flows. First, we induce controlled separation in an otherwise unseparated channel flow; the motivation for such a procedure is mixing enhancement as discussed by Wang *et al.*[16] Second, we reduce the reattachment length behind a backward-facing step by inducing controlled reattachment closer to the step.

II. SETUP

A. The wall-shear equation

We consider an incompressible velocity field $\mathbf{v}(\mathbf{x},t)=[u(x,y,t),v(x,y,t)]$ defined on a two-dimensional spatial domain $\mathcal{D}$. We assume that a segment of the boundary of $\mathcal{D}$ lies on the $y=0$ axis. On this boundary segment, $\mathbf{v}$ is assumed to satisfy the no-slip boundary conditions

$$u(x,0,t)=v(x,0,t)=0. \tag{1}$$

We further assume that $\mathbf{v}$ satisfies the two-dimensional incompressible Navier-Stokes equations

$$\begin{aligned} u_t+u_xu+u_yv&=-\frac{1}{\rho}p_x+\nu(u_{xx}+u_{yy}),\\ v_t+v_xu+v_yv&=-\frac{1}{\rho}p_y+\nu(v_{xx}+v_{yy}),\\ u_x+v_y&=0, \end{aligned} \tag{2}$$

where $p(x,y,t)$ denotes the pressure, and ν and ρ are the kinematic viscosity and the density of the fluid, respectively.

Subtracting the x-derivative of the second equation in (2) from the y-derivative of the first equation, we obtain the well-known vorticity-transport equation

$$\begin{aligned} &\partial_t(u_y-v_x)+u(u_{xy}-v_{xx})+v(u_{xx}+u_{yy})\\ &\quad=\nu(2u_{xxy}+u_{yyy}-v_{xxx}). \end{aligned} \tag{3}$$

Restricting (3) to the $x\in[0,L]$ section of the $y=0$ boundary and using the boundary conditions (1), we find that the wall shear $w(x,t)=u_y(x,0,t)$ satisfies the PDE

$$w_t=2\nu w_{xx}+F(x,t), \tag{4}$$

where

$$F(x,t)=\nu\frac{\partial^3u}{\partial y^3}(x,0,t). \tag{5}$$

With $\alpha_1(t)$ and $\alpha_2(t)$ denoting the wall shear at the endpoints of $[0,L]$, the initial and boundary conditions for the *wall-shear equation* (4) are given by

$$\begin{aligned} &w(0,t)=\alpha_1(t),\quad w(L,t)=\alpha_2(t),\\ &w(x,t_0)=w_0(x)=u_y(x,0,t_0). \end{aligned} \tag{6}$$

Assume now that a distributed array of wall-shear sensors is placed along the $[0,L]$ boundary segment, as shown in Fig. 1. Such a sensor array renders both $w_t(x,t)$ and $w_{xx}(x,t)$ up to errors determined by the sensors' sampling time and spatial resolution. We therefore regard the forcing term

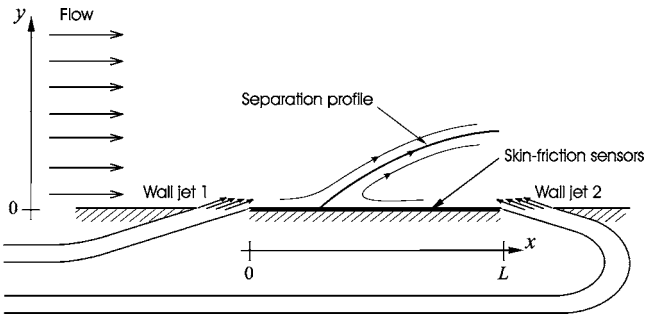

FIG. 1. Setting for separation control design, with distributed wall-shear sensors over the $[0,L]$ boundary section, and with two inclined jet actuators at the endpoints of the section.

$$F(x,t)=w_t-2\nu w_{xx} \tag{7}$$

as an available observed quantity.

We also assume that two actuators are placed close to the $x=0$ and $x=L$ boundary points. With these actuators present, we regard $\alpha_1(t)$ and $\alpha_2(t)$ as control outputs for the separation control law to be designed below. Figure 1 shows a possible physical realization of the actuators by two inclined wall-jets at the endpoints of $[0,L]$.

B. Solution of the wall-shear equation

With the observed term $F(x,t)$, (4) becomes a one-dimensional heat equation with distributed unsteady forcing. In order to solve the nonhomogeneous boundary-value problem (4)–(6), we first transfer it to a homogeneous one by letting

$$\begin{aligned} &\psi=w-G,\\ &G(x,t)=\frac{1}{L}[(L-x)\alpha_1(t)+x\alpha_2(t)]. \end{aligned} \tag{8}$$

Substitution of ψ into (4)–(6) then leads to the homogeneous problem

$$\begin{aligned} &\frac{\partial\psi}{\partial t}=2\nu\frac{\partial^2\psi}{\partial x^2}+F-\frac{\partial G}{\partial t},\\ &\psi(0,t)=0,\quad \psi(L,t)=0,\\ &\psi(x,t_0)=w_0(x)-G(x,t_0). \end{aligned} \tag{9}$$

Equation (9) admits the Fourier-series solution

$$\begin{aligned} \psi(x,t)=&\sum_{n=1}^{\infty}a_n(t_0)e^{-\xi_n(t-t_0)}\sin k_nx\\ &+\int_{t_0}^{t}\sum_{n=1}^{\infty}e^{-\xi_n(t-s)}[f_n(s)-g_n(s)]\sin k_nx\,ds, \end{aligned} \tag{10}$$

with

$$a_n(t_0) = \frac{2}{L}\int_0^L [w_0(x) - G(x,t_0)]\sin(n\pi x/L)\,dx,$$

$$f_n(t) = \frac{2}{L}\int_0^L F(x,t)\sin(n\pi x/L)\,dx,$$

$$g_n(t) = \frac{2}{L}\int_0^L \frac{\partial G}{\partial t}(x,t)\sin(n\pi x/L)\,dx$$

$$= \frac{2}{n\pi}[\dot{\alpha}_1(t) - \cos(n\pi)\dot{\alpha}_2(t)], \tag{11}$$

$$G_n(t) = \frac{2}{L}\int_0^L G(x,t)\sin(n\pi x/L)\,dx$$

$$= \frac{2}{n\pi}[\alpha_1(t) - \cos(n\pi)\alpha_2(t)],$$

$$\xi_n = 2\nu n^2\pi^2/L^2,$$

$$k_n = n\pi/L.$$

Equations (8) and (10) then yield the solution of the wall-shear equation (4) in the form

$$w(x,t) = \sum_{n=1}^{\infty}\left\{ w_n(t_0)e^{-\xi_n(t-t_0)} + \int_{t_0}^{t} e^{-\xi_n(t-s)}[f_n(s) + \xi_n G_n(s)]\,ds\right\}\sin k_n x, \tag{12}$$

where

$$w_n(t_0) = \frac{2}{L}\int_0^L w_0(x)\sin(n\pi x/L)\,dx.$$

Recall that $f_n(t)$, the Fourier coefficients of $F(x,t)$, are available from sensor data, and $G_n(t)$ depends only on the actuated wall shear values at $x=0,L$.

Suppose now that we measure $F(x,t)$ at a set of discrete times $\{t_k\}_{k=0}^{\infty}$ with the sampling time

$$\Delta = t_{k+1} - t_k;$$

we therefore obtain the Fourier amplitudes $f_n(t_k)$ from observations. Based on these observations, we update the actuator Fourier amplitudes $G_n(t)$ at times t_k, thus having

$$G_n(t) = G_n^k, \quad t \in [t_k, t_{k+1}), \quad k = 0,1,2,\ldots,$$

with the constants G_n^k yet to be determined as control outputs. Note that G_n^k, as functions of k, are not independent, because

$$G_n^k = \frac{2}{n\pi}[\alpha_1(t_k) - \cos(n\pi)\alpha_2(t_k)]. \tag{13}$$

C. Unsteady separation and reattachment criteria

As shown by Haller,[17] a sufficient criterion for fixed unsteady separation in an incompressible flow at the point $\mathbf{x}=(\gamma,0)$ is

$$\limsup_{t_0\to-\infty}\left|\int_{t_0}^{t} u_y(\gamma,0,s)ds\right| < \infty,$$
$$u_y(\gamma,0,t) < -c < 0, \tag{14}$$

for some constant $c>0$, and for all times $t<t_0$.

The first of these conditions ensures that material lines anchored at the separation point remain transverse to the boundary for all backward times. By contrast, wall-based material lines away from separation points align with the wall in backward time. The second condition in (14) ensures that fluid particles are ejected from the point $\mathbf{x}=(\gamma,0)$, thereby distinguishing $\mathbf{x}$ from reattachment points that also satisfy the first condition in (14).

As noted by Haller,[17] the $t_0\to-\infty$ limit in the first condition in (14) can be replaced by $t\to\infty$ with $t_0\leqslant t$ kept fixed. This modification is justified by the boundedness of separation profiles away from the wall in forward time. Furthermore, as proved by Kilic *et al.*,[18] it is sufficient if the second (14) holds in an average sense. These two observations lead to the modified separation criterion

$$\limsup_{t\to\infty}\left|\int_{t_0}^{t} u_y(\gamma,0,s)\,ds\right| < \infty,$$
$$\lim_{t\to\infty}\frac{1}{t-t_0}\int_{t_0}^{t} u_{xy}(\gamma,0,s)\,ds < -c < 0, \tag{15}$$

which is the principle underlying our separation controller design below.

Haller[17] also shows that a reattachment point exists at $x=\gamma$ if

$$\limsup_{t_0\to-\infty}\left|\int_{t_0}^{t} u_y(\gamma,0,s)\,ds\right| < \infty,$$
$$u_{xy}(\gamma,0,t) > c > 0, \tag{16}$$

for some constant $c>0$, and for all times $t<t_0$. Repeating the argument leading to the modified separation criterion (15), we obtain a modified *reattachment* criterion

$$\limsup_{t\to\infty}\left|\int_{t_0}^{t} u_y(\gamma,0,s)\,ds\right| < \infty,$$
$$\lim_{t\to\infty}\frac{1}{t-t_0}\int_{t_0}^{t} u_{xy}(\gamma,0,s)\,ds > c > 0. \tag{17}$$

As we shall see, the separation controller we propose below is also able to control reattachment by enforcing (17) at prescribed locations.

III. SEPARATION CONTROLLER DESIGN

We seek to enforce conditions (15) at time t_{m+1}, using wall-shear values measured up to time t_m. Specifically, we select the actuator strengths at time t_m to ensure

$$\int_{t_0}^{t_m} w(\gamma,t)\,dt + \int_{t_m}^{t_{m+1}} w^*(\gamma,t)\,dt = 0,$$
$$\int_{t_0}^{t_m} w_x(\gamma,t)\,dt + \int_{t_m}^{t_{m+1}} w_x^*(\gamma,t)\,dt = -\beta(t_{m+1}-t_0), \tag{18}$$

where $w^*(x,t)$ denotes an estimated value for $w(x,t)$ over the future time interval $[t_m,t_{m+1})$, and $\beta>0$ denotes a preselected constant. By (17), the control principle (18) is equally valid for generating reattachment at $x=\gamma$, provided that we select $\beta<0$.

To obtain an estimated wall-shear distribution $w^*(x,t)$, we fix the sampled value of $f_n(t_m)$ throughout the time interval $[t_m,t_{m+1})$ in formula (12). Using the step function

$$f_n^*(s) = f_n[s-(s \bmod \Delta)],$$

and replacing t_0 by t_m in (12), we then obtain the estimate

$$w^*(x,t) = \sum_{n=1}^{\infty}\left\{ w_n(t_m)e^{-\xi_n(t-t_m)} + \int_{t_m}^{t} e^{-\xi_n(t-s)} f_n^*(s)\,ds + \int_{t_m}^{t} e^{-\xi_n(t-s)}\xi_n G_n(s)\,ds \right\}\sin k_n x \tag{19}$$

to be used in the control principle (18).

When solved for the control outputs $\alpha_i(t_m)$, Eq. (19) yields the control law

$$\alpha_1(t_m) = \frac{DE_m - BF_m}{AD-BC}, \quad \alpha_2(t_m) = \frac{AF_m - CE_m}{AD-BC}, \tag{20}$$

with

$$A = \sum_{n=1}^{\infty}\frac{2}{n\pi}\left(\Delta - \frac{1-e^{-\xi_n\Delta}}{\xi_n}\right)\sin k_n\gamma,$$

$$B = -\sum_{n=1}^{\infty}\frac{2}{n\pi}\cos(n\pi)\left(\Delta - \frac{1-e^{-\xi_n\Delta}}{\xi_n}\right)\sin k_n\gamma,$$

$$C = \sum_{n=1}^{\infty} k_n\frac{2}{n\pi}\left(\Delta - \frac{1-e^{-\xi_n\Delta}}{\xi_n}\right)\cos k_n\gamma,$$

$$D = -\sum_{n=1}^{\infty} k_n\frac{2}{n\pi}\cos(n\pi)\left(\Delta - \frac{1-e^{-\xi_n\Delta}}{\xi_n}\right)\cos k_n\gamma,$$

and with

$$E_m = -\int_{t_0}^{t_m} w(\gamma,t)dt - \sum_{n=1}^{\infty}\left[w_n(t_m)\frac{1-e^{-\xi_n\Delta}}{\xi_n} + \frac{f_n(t_m)}{\xi_n}\left(\Delta - \frac{1-e^{-\xi_n\Delta}}{\xi_n}\right)\right]\sin k_n\gamma,$$
$$F_m = -\int_{t_0}^{t_m}[\beta + w_x(\gamma,t)]dt - \beta\Delta - \sum_{n=1}^{\infty} k_n\left\{ w_n(t_m)\frac{1-e^{-\xi_n\Delta}}{\xi_n} + \frac{f_n(t_m)}{\xi_n}\left(\Delta - \frac{1-e^{-\xi_n\Delta}}{\xi_n}\right)\right\}\cos k_n\gamma. \tag{21}$$

We give more details on deriving these formulae in Appendix A. We note that for the choice $\beta<0$, the above control law generates flow reattachment at $x=\gamma$.

The control principle (18) leading to (20) differs from the exact separation criterion (15). Nevertheless, as we show in Appendix B, the control law (20) will generate a fixed unsteady separation point satisfying (15) as long as $u_{yyyt}(x,0,t)$ remains continuously differentiable in x, and $u_{yyyxt}(x,0,t)$ remains uniformly bounded in t over the $[0,L]$ section of the boundary. In other words, as long as the control law (20) does not create a global instability with steadily growing velocity derivatives, the controller will generate a separation or reattachment point at the prescribed location $x=\gamma$. In practice, potential global instabilities can be avoided by putting bounds on the admissible actuator strengths.

Since the forcing term $F(x,t)$ in the wall-shear equation (4) is a priori unknown, an explicit stability analysis of the control law (20) is not possible. The results of Appendix B, however, guarantee a certain robustness of the controller: as long as the appropriate derivatives of the controlled velocity field remain uniformly bounded under some disturbance, the controller will create separation exactly at the required location $\mathbf{x}=(\gamma,0)$.

IV. IMPLEMENTATION OF THE SEPARATION CONTROLLER

Here we discuss the implementation of the control law (20) in numerical simulations of Navier-Stokes flows. To emulate the inevitable errors and inaccuracies of an experimental implementation, we do not pursue maximal accuracy in computing the derivatives and integrals of the wall-shear field. At the same time, we do add an additional proportional gain factor to our controller, as well as a local feedback loop on the actuator outputs, to secure the stability of the closed-loop flow.

A. Approximations

Instead of using continuously measured wall-shear data, we only use $w(x,t)$ measured at multiples of the sampling time Δ. As a result, we have

$$\int_{t_0}^{t_m} w(\gamma,t)\,dt \approx \Delta\sum_{k=1}^{m} w(\gamma,t_k),$$

$$\int_{t_0}^{t_m} [\beta w_x(\gamma,t)]\,dt \approx \Delta\left[m\beta + \sum_{k=1}^{m} w_x(\gamma,t_k)\right]$$

in (21).

In calculating $F(x,t)=\nu u_{yyy}(x,t)$ from (7), we use one-sided finite differencing in t and centered finite-differencing in x. The time step for the former is the sampling time Δ, which will be set to $\Delta=1$ s in our simulations (see below for motivation). The spatial resolution for finite-differencing will be set to $\delta=0.02$ m, which falls well within the spacing of available wall-shear sensor arrays.

Finally, in computing the control law (20), we truncate the arising Fourier series at the order $n=14$. In the examples considered below, this truncation results in a relative error below 2%.

B. Additional proportional gain

Recall that $F(x,t)$ in the wall-shear equation (4) depends on $w(x,t)$ in an unknown fashion. Actuation of the wall-shear field, therefore, may result in a substantial change of $F(x,t)$, which in turn may prompt a strong reaction from the controller, leading to instability. To reduce the risk of such an instability, we include an additional proportional gain term $\lambda<1$ in the control law (20), to obtain the modified controller.

$$\alpha_1(t_m)=\lambda\frac{DE_m-BF_m}{AD-BC},\quad \alpha_2(t_m)=\lambda\frac{AF_m-CE_m}{AD-BC}. \tag{22}$$

Unlike our original control principle (18), the modified controller (22) does not insist on making the wall-shear integral vanish in one time step. Rather, for $\lambda<1$, the controller has a damped reaction that results in greater stability.

A separation controller of the type (22) is inevitably unstable for $\lambda=1$ whenever delay effects associated with flow inertia are present.[20] The controller, however, becomes increasingly stable for larger sampling times and for lower values of the gain λ. Motivated by these results, we selected the relatively large sampling time $\Delta=1$ s, and the low gain value $\lambda=\mathcal{O}(10^{-3})$, which resulted in smooth control action in all our examples. This choice of parameters would normally cause slow convergence for the controller, but we accelerate the convergence by selecting large values for the prescribed separation (or reattachment) strength β.

C. Actuator modeling and control

To generate the actuator outputs required by the controller, we use two inclined wall jets, as shown in Fig. 1. The inclination angle of the jets is $\tan^{-1}(0.1)$, which ensures blowing or suction almost parallel to the wall. Before leaving the wall, the jets' cross section has width 0.01 m; the jet orifices are located at $x=0$ m and $x=L=1$ m. We have performed a series of open-loop simulations with zero background flow to obtain an approximation for the required jet speed $\mathbf{v}_{jet}$ as a function of the wall shear to be generated at the actuators. For near-zero blowing, we have found no clear trend, but for 1 m/s$<|\mathbf{v}_{\text{jet}}|<$10 m/s, we observed a near-linear relationship between the open-loop blowing strengths and the induced wall shear. We approximate this relationship by the formula

$$|\mathbf{v}^i_{\text{jet}}|=0.00572\tilde{u}^i_y,\quad i=1,2, \tag{23}$$

where $\tilde{u}^1_y=w(0,t)$, and $\tilde{u}^2_y=-w(L,t)$.

In the closed-loop system, the relationship (23) is altered by the unsteady background flow that interacts with the actuator flow in a nonlinear fashion. Nevertheless, for intermediate Reynolds numbers, we still find (23) an adequate first-order prediction for the required blowing strength.

To increase the precision of the above prediction, we also implement a local proportional feedback loop on the intended and measured values of wall shear at the jet outlets (see Fig. 2). If the error between the wall shear generated by the linear actuator law (23) and that required by the control law (22) exceeds 10%, the local feedback loop increases (or decreases) the proportionality constant in front of $\tilde{u}^i_y$ in (23).

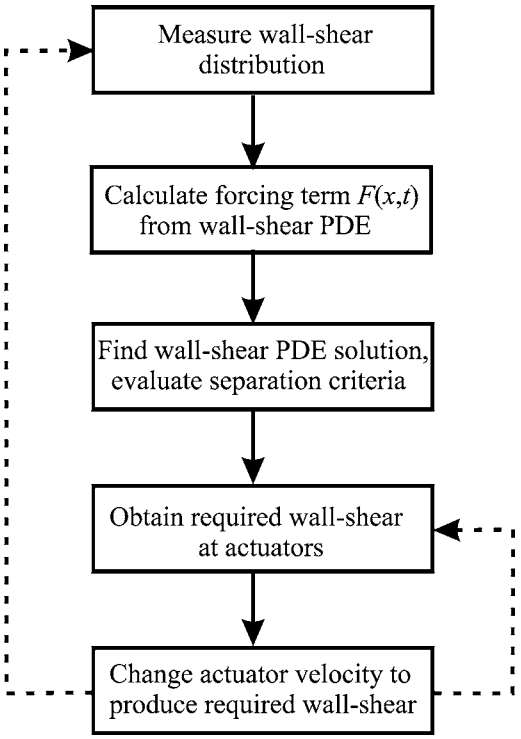

FIG. 2. An outline of our feedback control algorithm, showing the additional local feedback loop on the actuators.

V. NUMERICAL EXAMPLES

In our simulations, we used the two-dimensional FLUENT solver for incompressible laminar flow, with added external routines implementing the controller. For the fluid, we used air with $\rho=1.225$ kg/m^3 and $\mu=1.77\times10^{-5}$ kg/(m s).

A. Control of steady separation in a channel

As our first example, we consider a channel flow with the uniform inflow boundary condition $u_{\text{in}}=0.03$ m/s upstream (see Fig. 3). The height of the channel is $H=0.5$ m,

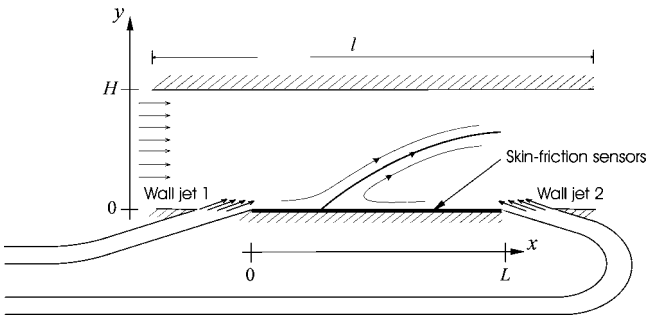

FIG. 3. Geometry for separation control in a steady channel flow.

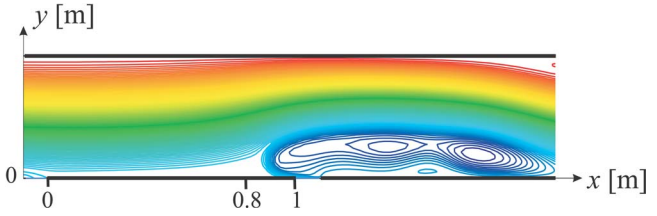

FIG. 5. Separation created by feedback control in the steady channel flow for $\gamma=0.8$ m. The separation point and separation profile are visualized by streamlines.

yielding the Reynolds number $\mathrm{Re}=10^3$; the channel length is $l=6$ m. For the boundary section $[0,L]$ in our control scheme, we select $L=1$ m; this means that the two inclined-jet actuators are placed at the endpoints of the $[0,1]$ interval on the lower boundary of the channel (see Fig. 3).

In this unseparated flow, we seek to introduce a fixed separation point on the lower boundary at $x=\gamma=0.8$ m. We select the separation strength parameter $\beta=1.2\times10^4$ 1/ms and the gain factor $\lambda=10^{-4}$ in order to obtain smoothly varying control action (cf. Sec. IV B).

Figure 4 shows the time-history of the wall shear and its integral at the intended separation point in the closed-loop system. Also shown are the actuator outputs α_i determined by the control law (22).

The streamlines in Fig. 5 confirm the creation of a separation point at $x=0.8$ m.

B. Control of unsteady separation in a channel

For the channel studied above, we now set the inflow boundary condition to $u_{\mathrm{in}}=0.03+0.015\sin ft$ m/s, with the oscillation frequency $f=0.05$ Hz; the Reynolds number is again $\mathrm{Re}=10^3$. The desired separation point is now at $\gamma=0.7$. We select the gain factor $\lambda=10^{-4}$ in the modified control law (20) and, in accordance with Sec. IV B, we set $\beta=10^4$ 1/ms.

Figures 6(a) and 6(b) show the variation of $u_y(\gamma,0,t)$ and $\int_0^t u_y(\gamma,0,s)\,ds$ in both the uncontrolled flow (dashed line) and the closed-loop flow (continuous line). By the separation criterion (15), Figure 6(b) shows the creation of fixed unsteady separation at $x=\gamma$. Figures 6(c) and 6(d) show the time-history of the actuator outputs.

Figure 7 confirms that unsteady separation is created by the controller at the desired location. Since the flow is unsteady, we visualize the separation location by releasing streaklines from the boundary. Note how the streaklines accumulate on a well-defined separation profile emanating from $x=\gamma=0.7$ m. By contrast, instantaneous streamlines and the point of zero wall shear move in a seemingly unrelated fashion.

C. Control of reattachment behind a backward-facing step

As our third numerical example, we consider a backward-facing step inside a channel of height $H=0.2$ m, with the top of the step located at $h=0.1$ m (see Fig. 8). The distance between the upstream wall-jet and the step is

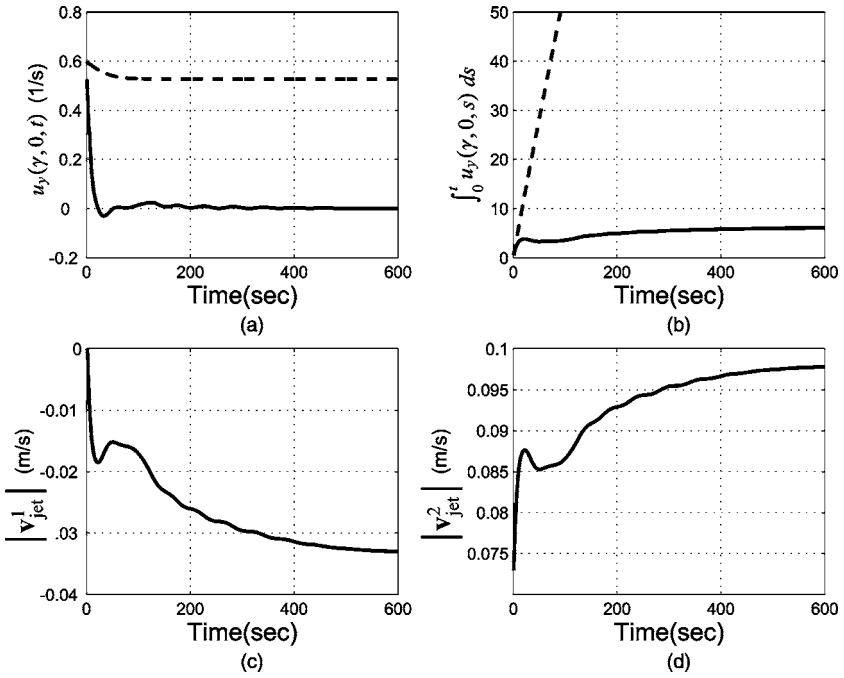

FIG. 4. Separation in the closed-loop steady channel flow. (a) Wall shear at the intended separation point $x=\gamma$. (dashed line: uncontrolled; solid line: closed loop). (b) Integral of the wall shear at $x=\gamma$ (dashed line: uncontrolled; solid line: closed loop). (c)–(d) Actuator outputs (mean speeds of wall jets).

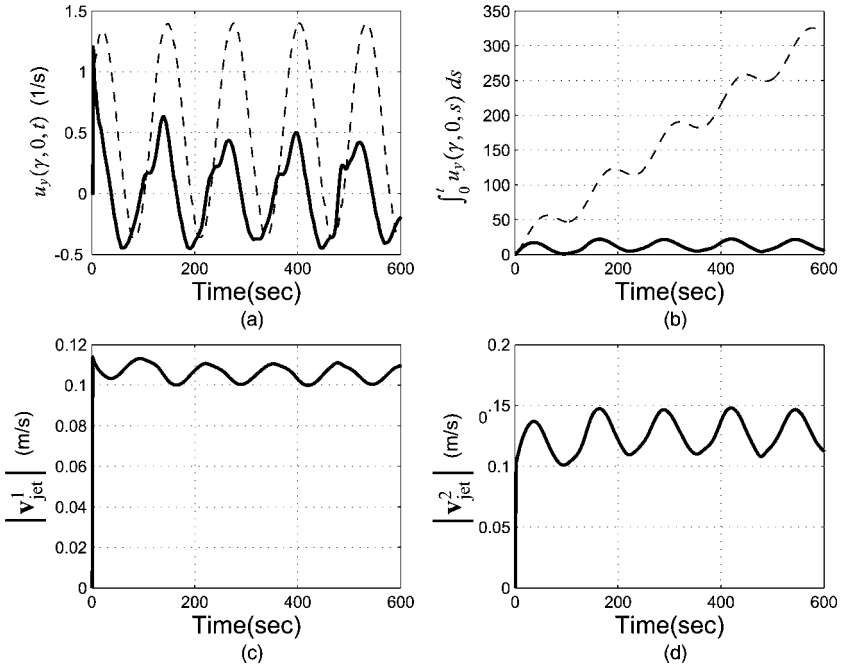

FIG. 6. Separation in the closed-loop unsteady channel flow. (a) Wall shear at the intended separation point $x=\gamma$ (b) Integral of the wall shear at $x=\gamma$. (c)–(d) Actuator outputs (mean speeds of wall jets).

$d=0.1$ m; the downstream wall-jet is located at $x=L=1$ m. The channel lengths upstream and downstream of the step are 0.5 m and 4 m.

We set the inflow velocity to $u_{\text{in}}=0.015$ m/s, which results in a Reynolds number of the order of 200. For higher Reynolds numbers, we found our actuator modeling scheme (Sec. IV C) inaccurate. The inaccuracy is the result of the predominant sucking action of the actuators, which affects the flow in a more complex fashion than blowing does. We also kept the Re=200 for physical reasons: for Reynolds numbers higher than 400, two-dimensional step simulations differ qualitatively from what is seen in the vertical midplane of the actual three-dimensional flow.[21]

As the uncontrolled simulation in Fig. 9 shows, the approximate location of reattachment is $x=0.3$ m. We seek to reduce the size of the recirculation zone by moving the reattachment point to $\gamma=0.2$ m. For the reattachment strength parameter, we select $\beta=-10$, and for the gain factor in the controller (22), we choose $\lambda=0.001$ following the discussion in Sec. IV B.

Figure 10 shows the wall shear and its integral, as well as the wall-shear gradient and its integral, evaluated at $x=\gamma$ in the closed-loop system; also shown are the actuator outputs as functions of time. Figures 10(b) and 10(d) confirm that the fixed unsteady reattachment conditions (17) are indeed enforced by the controller at $\gamma=0.2$.

We show the evolution of the wall-shear distribution behind the backward-facing step in Fig. 11. Finally, Fig. 12 shows the closed-loop velocity field and corresponding streaklines colored by the pressure distribution.

VI. CONCLUSIONS

We have developed a new approach to controlling separation on no-slip walls of two-dimensional flows that are incompressible near the boundary. Viewing the wall-shear distribution on the wall as the solution of an externally forced linear parabolic PDE, we control the location of unsteady separation or reattachment through the boundary conditions of the PDE.

Our controller assumes distributed wall-shear sensors, but requires actuation only at two discrete points on the boundary. By contrast, available (sub)optimal separation controllers for the Navier-Stokes equations require volume observations as well as volume controllers or distributed boundary controllers.[22] Furthermore, the controller developed here does not rely on reduced-order modeling or the extraction of dominant modes.

The above features make our control algorithm a promising candidate for experimental implementation. In such an implementation, arrays of recent optical wall-shear sensors can be deployed to obtain spatial resolutions below 15 μm without any calibration.[23] The frequency range of the same sensors is 1 kHz–10 MHz for Reynolds numbers up to 10^8. Thus, currently available spatial and temporal resolution for high-end wall-shear measurement greatly exceeds the resolution we assumed in our numerical examples ($\delta=0.02$ m and $\Delta=1$ *s*).

The numerical examples considered in this paper are limited to the Reynolds number regime 200–1000; higher-Reynolds-number flows are in principle amenable to the same approach, but require more accurate actuator modeling, more elaborate numerical simulation, and more attention to delay and sampling errors.

We have proved that our controller will generate the prescribed separation or reattachment point as long as appropriate derivatives of the velocity field remain uniformly bounded. Such uniform boundedness always holds in real-life flows if we impose bounds on the actuator strength. Imposing such bounds artificially, however, will change the control law we developed. The real question is, therefore, whether the flow remains uniformly bounded in the absence of saturated actuation.

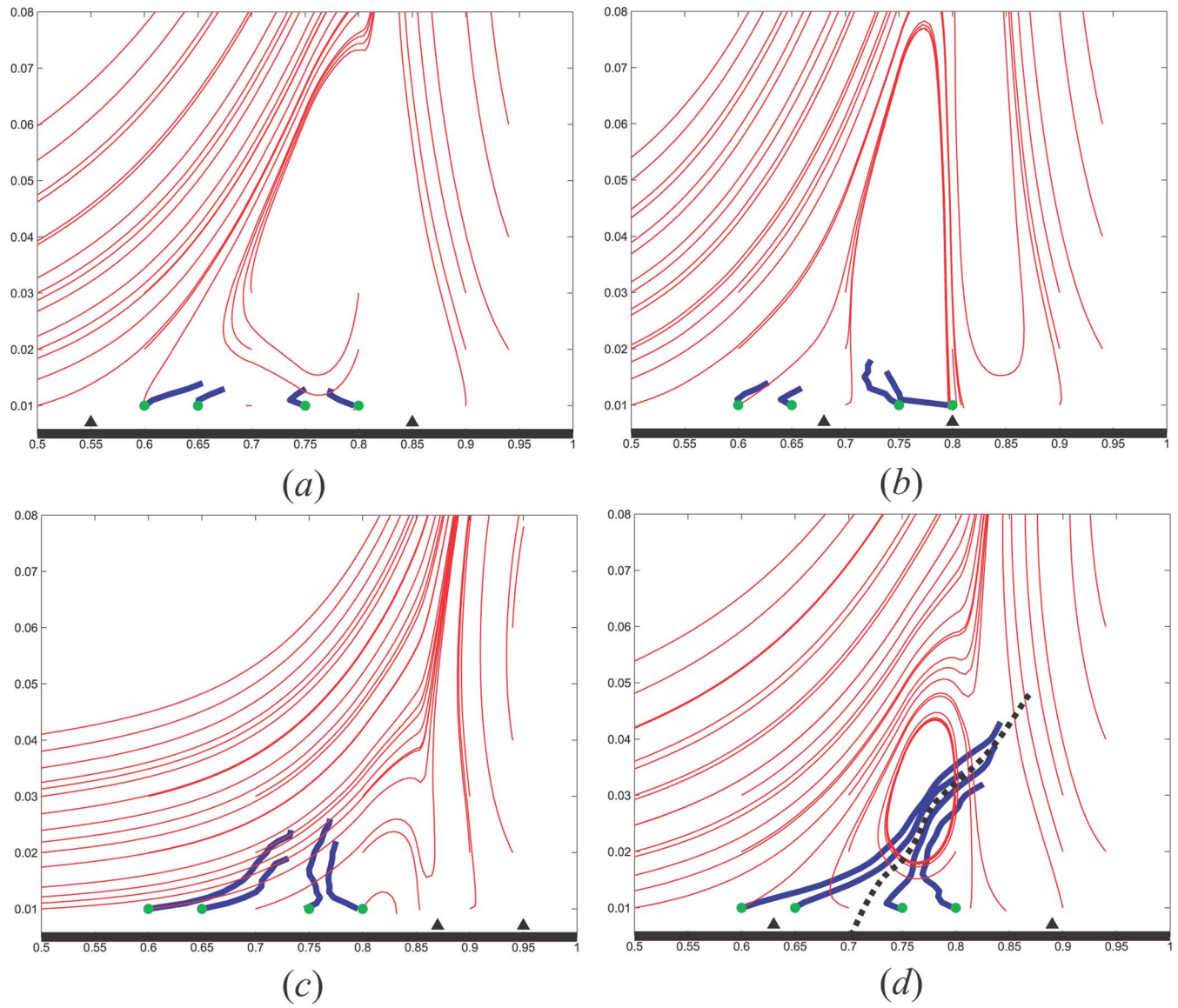

FIG. 7. Unsteady separation at $x=0.7$ m in the unsteady channel flow simulation, with the $x \in [0.5, 1.0]$ boundary domain shown. The images (a)–(d) show the evolution of four streaklines with the corresponding instantaneous streamline plots. Black triangles indicate instantaneous wall shear zeros. Dashed line indicates the unsteady separation profile (unstable manifold) inferred from the streakline geometry.

To guarantee uniform boundedness of the flow without bounding the actuation strength, we need a better understanding of the forcing term $F(x,t)$ in the wall-shear PDE (4). We are currently working to obtain a simplified evolution equation for $F(x,t)$ without solving the full Navier-Stokes equations. Recent results by Bewley and Protas[24] suggest that a leading-order model for $F(x,t)$ must include the wall-shear and the wall-pressure gradient.

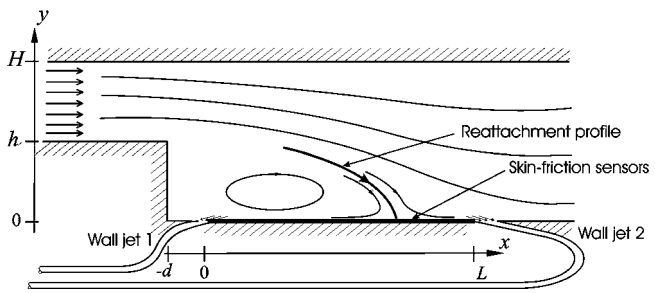

FIG. 8. Setup for reattachment control behind a backward-facing step (image is not to scale).

A limitation of the present approach is the lack of an estimate for convergence times. For some choices of the desired separation or reattachment point, we have observed curiously long settling times. The settling time should improve once the present proportional control scheme is extended to a proportional-integral-differential controller that also utilizes the integral and the derivative of the error term $\int_{t_0}^{t_{m+1}} w(\gamma,t)\, dt$. This extension is planned for future work.

A three-dimensional generalization of our results is nontrivial, because the boundary control of the corresponding two-dimensional forced wall-shear PDE is technically involved. Still, recent progress in the theory of three-

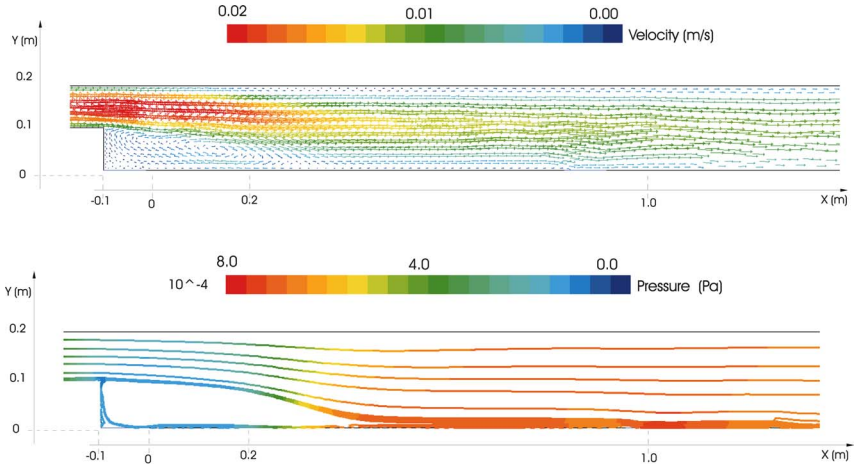

FIG. 9. Uncontrolled velocity field and streaklines colored by the pressure distribution in the backward-facing-step flow.

dimensional separation provides a strong analytical basis for a higher-dimensional extension.[25]

ACKNOWLEDGMENTS

We are grateful to Gustaav Jacobs for advice on numerical simulations and to Tom Peacock for information on wall-shear sensors. We also thank Tom Bewley, Miroslav Krstic, and Gilead Tadmor for useful discussions on flow control. Finally, we thank the anonymous referees for their comments and suggestions. This work was supported by AFOSR Grant No. F49620-03-1-0200 and NSF Grant No. DMS-04-04845.

APPENDIX A: DERIVATION OF CONTROL LAW

Here we derive the control law (20) from the control principle (18). First, we substitute the expression in (19) into

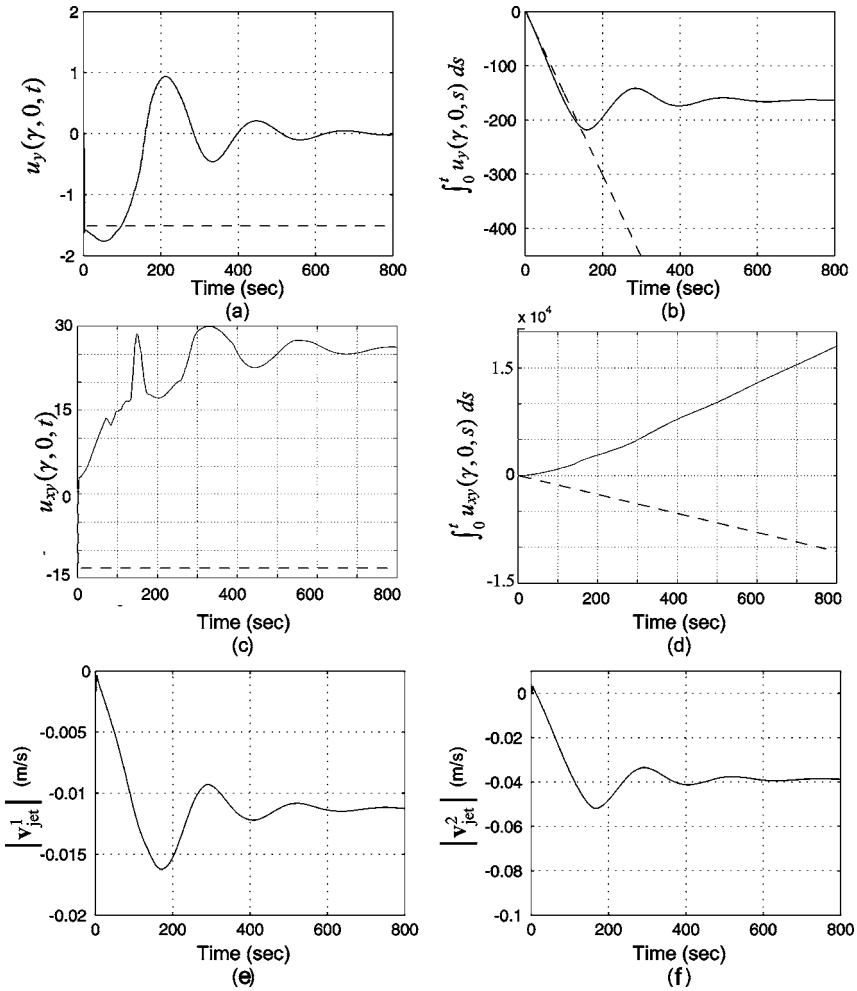

FIG. 10. Reattachment in the closed-loop backward-facing step flow. (a) Wall shear at $x=\gamma$ (dashed line: uncontrolled value). (b) Integral of the wall shear at $x=\gamma$ (dashed line: uncontrolled value). (c)–(d) Actuator outputs (mean speeds of wall jets).

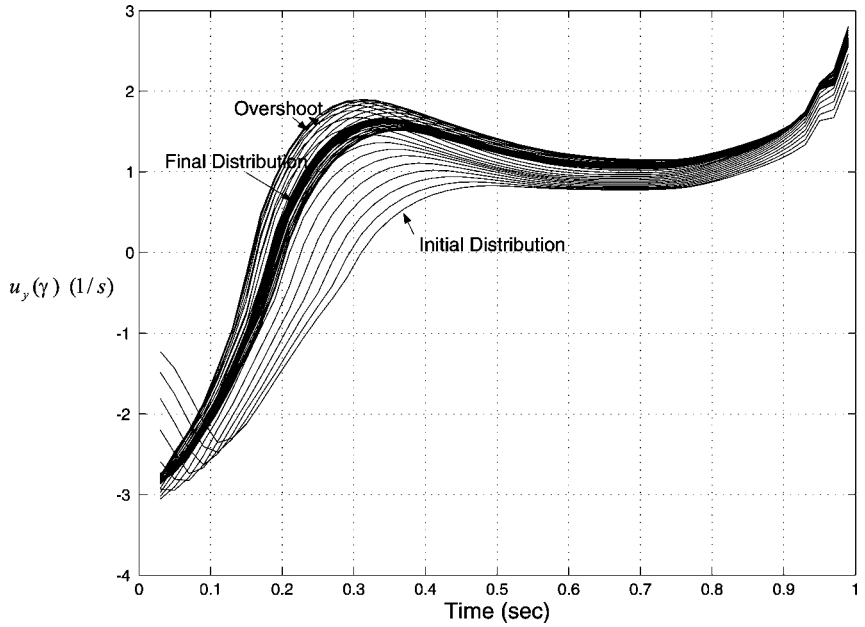

FIG. 11. Evolution of the wall-shear distribution behind the step in the controlled backward-facing step flow.

(18) to express the integrals $\int_{t_0}^{t_m} w(\gamma,t)dt$ and $\int_{t_0}^{t_m}[\beta + w_x(\gamma,t)]\,dt$ in the form

$$\begin{aligned}\int_{t_0}^{t_m} w(\gamma,t)\,dt &= -\int_{t_m}^{t_{m+1}} \left\{ \sum_{n=1}^{\infty} [w_n(t_m)e^{-\xi_n(t-t_m)} \right. \\ &\quad + \int_{t_m}^{t} e^{-\xi_n(t-s)} f_n^*(s)\,ds \\ &\quad \left. + \int_{t_m}^{t} e^{-\xi_n(t-s)} \xi_n G_n(s)\,ds \right] \sin k_n\gamma \Big\}\,dt \\ &= -\int_{t_m}^{t_{m+1}} \left\{ \sum_{n=1}^{\infty} \left[w_n(t_m)e^{-\xi_n(t-t_m)} \right. \right. \\ &\quad \left. \left. + \left(\frac{f_n(t_m)}{\xi_n} + G_n^m \right)(1-e^{-\xi_n(t-t_m)}) \right] \sin k_n\gamma \right\} dt, \end{aligned} \tag{A.1}$$

and

$$\begin{aligned}&\int_{t_0}^{t_m} [\beta + w_x(\gamma,t)]\,dt \\ &\quad = -\int_{t_m}^{t_{m+1}} \left\{ \beta + \sum_{n=1}^{\infty} k_n \left[w_n(t_m)e^{-\xi_n(t-t_m)} \right. \right. \\ &\qquad \left. \left. + \left(\frac{f_n(t_m)}{\xi_n} + G_n^m \right)(1-e^{-\xi_n(t-t_m)}) \right] \cos k_n\gamma \right\} dt. \end{aligned} \tag{A.2}$$

Evaluating the integrals on the right-hand sides of (A.1) and (A.2), we obtain

$$\begin{aligned}-\int_{t_0}^{t_m} w(\gamma,t)\,dt &= \sum_{n=1}^{\infty} \left[w_n(t_m)\frac{1-e^{-\xi_n\Delta}}{\xi_n} + \left(\frac{f_n(t_m)}{\xi_n} + G_n^m \right) \right. \\ &\quad \left. \times \left(\Delta - \frac{1-e^{-\xi_n\Delta}}{\xi_n} \right) \right] \sin k_n\gamma, \end{aligned}$$

$$\begin{aligned}&-\int_{t_0}^{t_m} [\beta + w_x(\gamma,t)]\,dt - \beta\Delta \\ &\quad = \sum_{n=1}^{\infty} k_n \left[w_n(t_m)\frac{1-e^{-\xi_n\Delta}}{\xi_n} + \left(\frac{f_n(t_m)}{\xi_n} + G_n^m \right) \right. \\ &\qquad \left. \times \left(\Delta - \frac{1-e^{-\xi_n\Delta}}{\xi_n} \right) \right] \cos k_n\gamma, \end{aligned}$$

which give

$$\begin{aligned}&\sum_{n=1}^{\infty} G_n^m \left(\Delta - \frac{1-e^{-\xi_n\Delta}}{\xi_n} \right) \sin k_n\gamma \\ &\quad = -\int_{t_0}^{t_m} w(\gamma,t)\,dt - \sum_{n=1}^{\infty} \left[w_n(t_m)\frac{1-e^{-\xi_n\Delta}}{\xi_n} \right. \\ &\qquad \left. + \frac{f_n(t_m)}{\xi_n} \left(\Delta - \frac{1-e^{-\xi_n\Delta}}{\xi_n} \right) \right] \sin k_n\gamma, \end{aligned}$$

$$\begin{aligned}&\sum_{n=1}^{\infty} k_n G_n^m \left(\Delta - \frac{1-e^{-\xi_n\Delta}}{\xi_n} \right) \cos k_n\gamma \\ &\quad = -\int_{t_0}^{t_m} [\beta + w_x(\gamma,t)]\,dt - \beta\Delta \\ &\qquad - \sum_{n=1}^{\infty} k_n \left[w_n(t_m)\frac{1-e^{-\xi_n\Delta}}{\xi_n} \right. \\ &\qquad \left. + \frac{f_n(t_m)}{\xi_n} \left(\Delta - \frac{1-e^{-\xi_n\Delta}}{\xi_n} \right) \right] \cos k_n\gamma. \end{aligned}$$

Substitution of (13) into the above equations yields

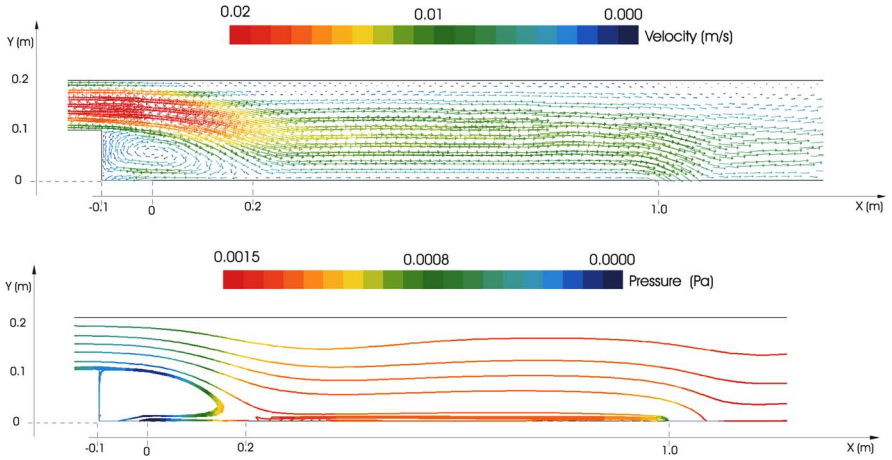

FIG. 12. Closed-loop velocity field and closed-loop streaklines colored by the pressure distribution in the backward-facing-step flow.

$$\alpha_1(t_m)\left[\sum_{n=1}^{\infty}\frac{2}{n\pi}\left(\Delta-\frac{1-e^{-\xi_n\Delta}}{\xi_n}\right)\sin k_n\gamma\right]-\alpha_2(t_m)\left[\sum_{n=1}^{\infty}\frac{2}{n\pi}\cos(n\pi)\left(\Delta-\frac{1-e^{-\xi_n\Delta}}{\xi_n}\right)\sin k_n\gamma\right]$$
$$=-\int_{t_0}^{t_m}w(\gamma,t)dt-\sum_{n=1}^{\infty}\left[w_n(t_m)\frac{1-e^{-\xi_n\Delta}}{\xi_n}+\frac{f_n(t_m)}{\xi_n}\left(\Delta-\frac{1-e^{-\xi_n\Delta}}{\xi_n}\right)\right]\sin k_n\gamma,$$
$$\alpha_1(t_m)\left[\sum_{n=1}^{\infty}k_n\frac{2}{n\pi}\left(\Delta-\frac{1-e^{-\xi_n\Delta}}{\xi_n}\right)\cos k_n\gamma\right]-\alpha_2(t_m)\left[\sum_{n=1}^{\infty}k_n\frac{2}{n\pi}\cos(n\pi)\left(\Delta-\frac{1-e^{-\xi_n\Delta}}{\xi_n}\right)\cos k_n\gamma\right]$$
$$=-\int_{t_0}^{t_m}[\beta+w_x(\gamma,t)]\,dt-\beta\Delta-\sum_{n=1}^{\infty}k_n\left[w_n(t_m)\frac{1-e^{-\xi_n\Delta}}{\xi_n}+\frac{f_n(t_m)}{\xi_n}\left(\Delta-\frac{1-e^{-\xi_n\Delta}}{\xi_n}\right)\right]\cos k_n\gamma. \tag{A.3}$$

With the notation (21), system (A.3) becomes

$$\begin{pmatrix}A & B\\ C & D\end{pmatrix}\begin{pmatrix}\alpha_1(t_m)\\ \alpha_2(t_m)\end{pmatrix}=\begin{pmatrix}E_m\\ F_m\end{pmatrix},$$

whose solution is

$$\begin{pmatrix}\alpha_1(t_m)\\ \alpha_2(t_m)\end{pmatrix}=\begin{pmatrix}A & B\\ C & D\end{pmatrix}^{-1}\begin{pmatrix}E_m\\ F_m\end{pmatrix}=\begin{pmatrix}\dfrac{DE_m-BF_m}{AD-BC}\\ \dfrac{AF_m-CE_m}{AD-BC}\end{pmatrix},$$

which proves (20).

APPENDIX B: CONVERGENCE OF CONTROLLER

The actuated value of the wall-shear integral at $x=\gamma$ and at time t_{m+1} is

$$\int_{t_0}^{t_{m+1}}w(\gamma,t)\,dt=\int_{t_0}^{t_m}w(\gamma,t)\,dt+\int_{t_m}^{t_{m+1}}w(\gamma,t)\,dt=-\int_{t_m}^{t_{m+1}}w^*(\gamma,t)\,dt+\int_{t_m}^{t_{m+1}}w(\gamma,t)\,dt$$
$$=\int_{t_m}^{t_{m+1}}\left(\sum_{n=1}^{\infty}\left\{\int_{t_m}^{t}e^{-\xi_n(t-s)}[f_n(s)-f_n^*(s)]\,ds\right\}\sin k_n\gamma\right)dt=\sum_{n=1}^{\infty}\left\{\int_{t_m}^{t_{m+1}}\int_{t_m}^{t}e^{-\xi_n(t-s)}[f_n(s)\right.$$
$$\left.-f_n^*(s)]\,ds\,dt\right\}\sin k_n\gamma=\sum_{n=1}^{\infty}\left\{\int_{t_m}^{t_{m+1}}\int_{s}^{t_{m+1}}e^{-\xi_n(t-s)}[f_n(s)-f_n^*(s)]\,dt\,ds\right\}\sin k_n\gamma$$
$$=\sum_{n=1}^{\infty}\left\{\int_{t_m}^{t_{m+1}}\frac{1-e^{-\xi_n(t_{m+1}-s)}}{\xi_n}[f_n(s)-f_n^*(s)]\,ds\right\}\sin k_n\gamma.$$

We therefore obtain

$$\limsup_{m\to\infty}\left|\int_{t_0}^{t_{m+1}} w(\gamma,t)\,dt\right| = \limsup_{m\to\infty}\left|\sum_{n=1}^{\infty}\left\{\int_{t_m}^{t_{m+1}}\frac{1-e^{-\xi_n(t_{m+1}-s)}}{\xi_n}[f_n(s)-f_n^*(s)]\,ds\right\}\sin k_n\gamma\right|$$

$$\leqslant \limsup_{m\to\infty}\sum_{n=1}^{\infty}\left[\int_{t_m}^{t_{m+1}}\frac{1-e^{-\xi_n(t_{m+1}-s)}}{\xi_n}|f_n(s)-f_n^*(s)|ds\right]$$

$$\leqslant \limsup_{m\to\infty}\sum_{n=1}^{\infty}\max_{t\in[t_m,t_{m+1}]}|\dot{f}_n(t)|\Delta\left(\frac{\Delta}{\xi_n}-\frac{1-e^{-\xi_n\Delta}}{\xi_n^2}\right)\leqslant\Delta\sum_{n=1}^{\infty}\limsup_{t\to\infty}|\dot{f}_n(t)|\left(\frac{\Delta}{\xi_n}-\frac{1-e^{-\xi_n\Delta}}{\xi_n^2}\right). \tag{B.1}$$

If $F_t(x,t)$ is of class C^r in x, then for any fixed t, its Fourier coefficients obey estimates of the form

$$|\dot{f}_n(t)|\leqslant C(t)n^{-r}, \tag{B.2}$$

where $C(t)$ is a positive function of time. In that case, we obtain

$$\Delta\sum_{n=1}^{\infty}\limsup_{t\to\infty}|\dot{f}_n(t)|\left(\frac{\Delta}{\xi_n}-\frac{1-e^{-\xi_n\Delta}}{\xi_n^2}\right)\leqslant\Delta\sum_{n=1}^{\infty}\frac{1}{n^r}\frac{C_0\Delta}{\xi_n}=\frac{C_0\Delta^2L^2}{2\nu\pi^2}\sum_{n=1}^{\infty}\frac{1}{n^{r+2}}<\infty,$$

provided that $r\geqslant 0$ and $C(t)$ is uniformly bounded in t. Note that for any fixed n, $|\dot{f}_n(t)|$, and hence $C(t)$ remains uniformly bounded in t if $F_t(x,t)$ remains uniformly bounded in t.

We thus conclude that the controller (A.1) creates a wall-shear distribution satisfying the first separation condition in (15) if $\partial_t u_{yyy}(x,0,t)$ is continuous in x and uniformly bounded in t over the $[0,L]$ section of the boundary.

To see that the second condition in (15) is also enforced by the controller, note that the actual value of the wall-shear-gradient integral between t_m and t_{m+1} is

$$\int_{t_0}^{t_{m+1}} w_x(\gamma,t)\,dt=\int_{t_0}^{t_m} w_x(\gamma,t)\,dt+\int_{t_m}^{t_{m+1}} w_x(\gamma,t)\,dt$$

$$=-\beta(t_{m+1}-t_0)+\int_{t_m}^{t_{m+1}}[w_x(\gamma,t)-w_x^*(\gamma,t)]\,dt$$

$$=-\beta(m+1)\Delta+\int_{t_m}^{t_{m+1}}\left(\sum_{n=1}^{\infty}k_n\left\{\int_{t_m}^{t}e^{-\xi_n(t-s)}[f_n(s)-f_n^*(s)]\,ds\right\}\cos k_n\gamma\right)dt. \tag{B.3}$$

Proceeding as in (B.1) and assuming again that $F_{yt}(x,t)$ is C^r in x, we find that

$$\limsup_{m\to\infty}\left|\int_{t_m}^{t_{m+1}}\left(\sum_{n=1}^{\infty}k_n\left\{\int_{t_m}^{t}e^{-\xi_n(t-s)}[f_n(s)-f_n^*(s)]\,ds\right\}\cos k_n\gamma\right)dt\right|$$

$$\leqslant\limsup_{m\to\infty}\sum_{n=1}^{\infty}k_n\left|\int_{t_m}^{t_{m+1}}\frac{1-e^{-\xi_n(t_{m+1}-s)}}{\xi_n}[f_n(s)-f_n^*(s)]\,ds\right|$$

$$\leqslant\limsup_{m\to\infty}\sum_{n=1}^{\infty}\max_{t\in[t_m,t_{m+1}]}|\dot{f}_n(t)|k_n\Delta\left(\frac{\Delta}{\xi_n}-\frac{1-e^{-\xi_n\Delta}}{\xi_n^2}\right)$$

$$=\Delta\sum_{n=1}^{\infty}\limsup_{t\to\infty}|\dot{f}_n(t)|k_n\left(\frac{\Delta}{\xi_n}-\frac{1-e^{-\xi_n\Delta}}{\xi_n^2}\right)\leqslant\Delta\sum_{n=1}^{\infty}\frac{k_n}{n^r}\frac{C_0\Delta}{\xi_n}=\frac{C_0\Delta^2L}{2\nu\pi}\sum_{n=1}^{\infty}\frac{1}{n^{r+1}}<\infty \tag{B.4}$$

for some C_0, provided that $r \geqslant 1$ and $C(t)$ remains uniformly bounded for all t and all n. Under these conditions, (B.3) and (B.4) give

$$\lim_{m\to\infty} \frac{1}{t_{m+1}-t_0}\int_{t_0}^{t_{m+1}} w_x(\gamma,t)\,dt$$
$$= \lim_{m\to\infty} \frac{1}{t_{m+1}-t_0}\int_{t_0}^{t_m} w_x(\gamma,t)\,dt$$
$$+ \lim_{m\to\infty} \frac{1}{t_{m+1}-t_0}\int_{t_m}^{t_{m+1}} w_x(\gamma,t)\,dt$$
$$= \lim_{m\to\infty} \frac{-\beta\Delta m}{(m+1)\Delta} = -\beta,$$

showing that the second condition in the separation criterion (15) also holds.

[1] D. Greenblatt and I. J. Wygnanski, "The control of flow separation by periodic excitation," Prog. Aerosp. Sci. **36**, 487 (2000).
[2] A. Seifert, A. Darabi, and I. Wygnanski, "Delay of airfoil stall by periodic excitation," J. Aircr. **33**, 691 (1996).
[3] M. Amitay, D. Pitt, and A. Glezer, "Separation control in duct flows," AIAA J. **39**, 616 (2002).
[4] J. C. S. Lai, J. Yue, and M. F. Platzer, "Control of backward-facing step flow using a flapping foil," Exp. Fluids **32**, 44 (2002).
[5] S. Narayanan and A. Banaszuk, "Experimental study of a novel active separation control approach." AIAA Paper 2003–0060 (2003).
[6] S. H. Feakins, D. G. MacMartin, and R. M. Murray, "Dynamic separation control in a low-speed asymmetric diffuser with varying downstream boundary conditions," AIAA Paper 2003-4161 (2003).
[7] T. Suzuki, T. Colonius, and S. Pirozzoli, "Vortex shedding in a two-dimensional diffuser: theory and simulation of separation control by periodic mass injection," J. Fluid Mech. **520**, 187 (2004).
[8] I. Wygnanski, "The variables affecting the control of separation by periodic excitation," AIAA Paper 2004–2505 (2004).
[9] B. G. Allan, J.-N. Juang, D. L. Raney, A. Seifert, L. G. Pack, D. E. Brown, "Closed-loop separation control using oscillatory flow excitation," ICASE Technical Rep. 2000-32 (2000).
[10] B. D. Coller, B. R. Noack, S. Narayanan, A. Banaszuk, and A. Khibnik, "Reduced-basis model of active separation control in planar diffuser flow," AIAA Paper 2000-2562 (2000).
[11] T. Suzuki, T. Colonius, and D. G. MacMartin, "Closed-loop control of vortex shedding in a separated diffuser using an inverse method," AIAA Paper 2004-0577 (2004).
[12] J. Gerhard, M. Pastoor, R. King, B. R. Noack, A. Dillmann, M. Morzyński, and G. Tadmor, "Model-based control of vortex shedding using low-dimensional Galerkin models", AIAA Paper 2003-4262 (2003).
[13] S. Siegel, C. Cohen, and T. McLaughlin, "Experimental variable gain feedback control of a circular cylinder wake," AIAA Paper 2004-2611 (2004).
[14] R. King, R. Becker, M. Garwon, and L. Henning, "Robust and adaptive closed-loop control of separated shear flows," AIAA Paper 2004-2519 (2004).
[15] L. Prandtl, "Über Flüssigkeitsbewegung bei sehr kleiner Reibung," Int. Math. Kongr., Heidelberg, 1904, Verh. III, pp. 484.
[16] Y. Wang, G. Haller, A. Banaszuk, G. Tadmor, "Closed-loop Lagrangian separation control in a bluff body shear flow model," Phys. Fluids **15**, 2251 (2003).
[17] G. Haller, "Exact theory of unsteady separation for two-dimensional flows," J. Fluid Mech. **512**, 257 (2004).
[18] M. S. Kilic, G. Haller, and A. Neishtadt, "Unsteady fluid flow separation by the method of averaging," Phys. Fluids **17**, 067104 (2005).
[19] T. Peacock, R. Coral, and G. Haller, "Experimental validation of the kinematic theory of unsteady separation," AIAA Paper 2005-4903 (2005).
[20] Such a controller is described by T. Insperger, F. Lekien, H. Salman, G. Stépán, and G. Haller, "Control of separation point in periodic flows including delay effects" Proceedings of the IFAC Workshop on Periodic Control Systems, Yokohama, Japan, 2004.
[21] G. Biswas, M. Breuer, and F. Durst, "Backward-facing step flows for various expansion ratios at low and moderate Reynolds numbers," Trans. ASME **126**, 362 (2004).
[22] H. Choi, M. Hinze, and K. Kunish, "Instantaneous control of backward-facing step flows," Appl. Numer. Math. **31**, 133 (1999).
[23] D. Fourguette, D. Modarress, D. Wilson, M. Koochesfahani, and M. Gharib, "An optical MEMS-based shear stress sensor for high Reynolds number applications," AIAA Paper 2003-0742 (2003).
[24] T. Bewley, and B. Protas, "Skin friction and pressure: the 'footprints' of turbulence," Physica D **196**, 28 (2004).
[25] A. Surana, O. Grunberg, and G. Haller, "Exact theory of three-dimensional flow separation. Part I: Steady separation," J. Fluid Mech. (in press).